

# What controls the transition from shallow to deep convection?

CHIEN-MING WU\*, BJORN STEVENS AND AKIO ARAKAWA

*Department of Atmospheric and Oceanic Sciences University of California, Los Angeles, California*

Accepted by the Journal of the Atmospheric Sciences

November, 2008

---

\* *Corresponding author address:* Chien-Ming Wu, Department of Atmospheric and Oceanic Sciences,  
University of California, Los Angeles, California

E-mail: mog@atmos.ucla.edu

## ABSTRACT

In this study, a 2-D CSRM (Cloud-System Resolving Model) is used to assess the control mechanism for the transition from shallow to deep convection in the diurnal cycle over land. By comparing with a 3-D CSRM under conditions taken from the Large-scale Biosphere Atmosphere field study (in the Amazon), we show that the 2-D CSRM reproduces the main features evident in previous 3-D simulations reasonably well. To extract the essence of the transition from shallow to deep convection, we idealize the observed case to isolate two control parameters, the free troposphere stability and the relative humidity. The emergence of a distinct transition between shallow and deep convection shows that the convective transition is an intrinsic property of the system. A transition time is defined to evaluate the key mechanism of the transition. We show that the transition coincides with the time when the lapse rate of virtual potential temperature of the clouds becomes larger than that of the environment suggesting that transition happens when shallow clouds become, on average, buoyant. This suggests that given the opportunity, convection prefers to be shallow.

# 1. Introduction

One of the major characteristics of summer-time convective systems over land is their strong response to diurnal forcing. Typically the response is conceptualized as a progression through distinct phases, including the development of the dry convective boundary layer, the emergence of shallow cumulus clouds, the transition from shallow to deep cumulus clouds, the meso-scale organizations of deep cumulus clouds and (at times) the subsequent evolution of such systems as they draw moist air from low-level jets riding over stable boundary layers. It is difficult for large-scale models to capture this diurnal cycle because it depends almost entirely on sub-grid scale parameterizations which uncertainly represent the underlying physical processes. Model studies (Bechtold et al. 2004; Guichard et al. 2004; Betts and Jakob 2002) show that the surface precipitation generally develops a couple hours earlier in the morning in single column model (SCM) representations of the diurnal cycle over land as compared to observations, as the SCM representations consistently bypass the shallow cumulus phase. These studies concluded that the most challenging part of modeling the diurnal cycle over land is to represent the development of shallow cumulus and the transition toward deep convection. In this study, we endeavor to understand this transition and the particular role of shallow convection.

A major idea to emerge from previous studies emphasizes the negative effect of dry-air entrainment in quenching the buoyancy of convective plumes and hence the transition from shallow to deep convection. This idea follows from a number of cloud resolving model (CRM) studies which show that the development of deep convection depends on the moisture content of the free troposphere (Derbyshire et al. 2004; Kuang and Bretherton 2006; Chaboureau

et al. 2004). Derbyshire et al. (2004), for instance, documented the sensitivity of convective development to a wide range of environmental relative humidities (10% to 90%). Their results show that dry environment is unfavorable for deep convection as the entrainment of drier environmental air leads to stronger evaporative cooling and negative buoyancy. Kuang and Bretherton (2006) tested this argument in their simulation of the transition from shallow to deep cumulus convection by adding horizontally uniform values to the mixing ratio above 3 km when the shallow clouds start to develop so that the domain averaged mixing ratio matches that of the deep convection stage. Deep convection develops rapidly after moisture is added, thereby supporting the ideas put forth by Derbyshire et al. (2004). Chaboureau et al. (2004) also explained the development of deep convection through the moistening of the lower troposphere by shallow cumulus. In their study, deep convection only develops when the mean moisture near cloud base approaches saturation, further supporting the idea that the environmental humidity helps mediate the buoyancy of moist convective plumes.

Another way of maintaining the buoyancy of saturated updrafts is to shield them from deleterious effects of a dry environment, for instance, by making the clouds bigger. Khairoutdinov and Randall (2006) explored this issue in the context of high resolution simulations of the diurnal cycle as observed during the LBA (Large-Scale Biosphere-Atmosphere). Experiments in which the evaporation of rain was forbidden did not transit to deep convection. This result led them to hypothesize that cold pools, which are produced by downdrafts from congestus clouds, help organize larger scale circulations within the boundary layer, which in turn support the development of larger clouds. Because large clouds are less likely to be diluted by mixing with dry air in the mid-troposphere, they are expected to penetrate more deeply through the troposphere. Larger clouds then bring stronger precipitation, which

produces stronger cold pools and yet larger and more buoyant clouds.

The environmental temperature profile can also affect the buoyancy of convective plumes by modifying their level of free convection (LFC), and by implication, the initiation of deep convection (Ziegler et al. 1997; Ziegler and Rasmussen 1998; Johnson and Mapes 2001). Houston and Niyogi (2007) demonstrated the importance of the lapse rate of the environmental temperature for initiation of (or transition to) deep convection. Their results showed that deep convection fails to initiate even though the air parcel has reached its LFC and releases its thermal instability. For environments in which deep convection did not initiate, despite being conditionally unstable, the air parcel loses its buoyancy because the rate of increasing buoyancy due to parcel ascent is smaller than the rate of reducing buoyancy due to entrainment. Their results thus imply the existence of a critical lapse rate, somewhat more unstable than that required for conditionally unstable undiluted parcel ascent, to transition to deep convection.

The above arguments recognize the importance of maintaining the buoyancy of clouds for deep convection. Although they propose different pathways for overcoming such effects, i.e., making clouds big, or the environment more humid and less stable, one could imagine these processes playing a role. For the most part, however, the existing ideas on the ways in which humidity helps modulate the buoyancy of convective plumes is largely qualitative, serving to remind us of the important role it plays, while leaving concrete proposals for incorporating such effects to future work.

The need for advancing our ideas in this respect motivates our study. We rejoin these issues by first asking if a transition is an intrinsic property of the convection and its associated circulation system, rather than externally determined, for instance by particular features of

the sounding or surface forcing. Is the growth of the deep cumulus different from that of the shallow cumulus? If there is a significant difference, can we define a time for the transition, and then develop a theory that builds on the previous work to help understand what sets this timescale. In the following study, section 2 describes our methodology and its justification. The results of experiments designed to identify the transition time as a function of two control parameters are also presented. The temporal evolution and the quantitative definition of transition are presented in Section 3. The results outline a simple mechanism which we formulate in terms of a model for the transition time, and which we present in section 4. A summary and discussion are presented in section 5.

## 2. Model description and experiments

### *a. The model*

We analyze the transition simulated by a 2-D cloud-system resolving model (CSRM). An advantage of the 2-D CSRM is that it produces plausible simulations with much greater computational efficiency compared to the full 3-D CSRM. Hence a large ensemble of simulations can be performed with a fine resolution over a wide swath of parameter space. As far as the thermodynamic state is concerned, past studies (Tao et al. 1996; Redelsperger et al. 2000) show that 2-D simulations are compatible with the results from 3-D CSRMs.

The CSRM we used was originally developed by Krueger (1988) based on the anelastic equations in two dimensions. The model includes three kinds of physical parameterization: a radiation parameterization using a delta-four-stream approximation (Liou et al. 1988; Fu

et al. 1995) with six solar and twelve infrared bands, a bulk microphysical parameterization including cloud droplets, ice crystals, rain, snow, and graupel (Lin et al. 1983; Lord et al. 1984; Fu et al. 1995; Krueger et al. 1995a) and a turbulence parameterization based on a third-order closure (André et al. 1976, 1978; Krueger 1988). The turbulence parameterization uses a diagnostically determined turbulence length scale (Xu and Krueger 1991) and a turbulent-scale condensation (Chen 1991).

A distinguishing feature of this CSRM is the turbulence parameterization, which couples cloud-scale dynamics with boundary layer turbulence as well as the turbulence associated with clouds. It has long been recognized that subcloud layer turbulence is crucial in organizing convection (Krueger 1988). Proper representation of turbulence is important for simulating convection. Turbulence in clouds also plays an important role in entrainment of environmental air. Unlike boundary layer turbulence, it is difficult to capture the turbulent properties in cumulus clouds through observations. The third order turbulence parameterization better represents subgrid-scale processes than the more commonly used low-order closures. This model has been widely and successfully used to simulate clouds associated with the boundary layer such as stratocumulus (Moeng et al. 1996), trade cumulus (Krueger and Bergeron 1994; Lin and Arakawa 1997) and the transition from stratus to cumulus (Krueger et al. 1995b) as well as deep convection (Xu et al. 1992; Xu and Randall 1996; Fu et al. 1995). In tests performed in advance of this study, we also found that simulations incorporating this approach greatly reduced the sensitivity of the simulations to the grid spacing as compared to simulations based on more traditional, Smagorinsky-type, closures.

For all experiments presented in this study, the domain size is 154 km in the horizontal and 16 km in the vertical. The horizontal grid spacing is 100 m. In the vertical, we employ

a 155-layer vertically stretched grid (Krueger 1988) with a grid spacing of 50 m near the surface, 100 m near 5 km, and 150 m at the tropopause. A small random temperature perturbation is imposed on the lowest-layer for the initial 5 minutes in order to break the symmetry of the otherwise horizontally uniform initial state. The model is integrated over 6 hours with a 2-second time step. Ensemble results are obtained by averaging 16 simulations for each set of parameters, differentiated only by random seeds. We note that all of the features of the ensemble, which we discuss here, are also evident in individual realizations (simulations).

*b. The benchmark simulation*

We first perform a benchmark simulation of the transition from shallow to deep convection to evaluate the performance of the 2-D CSRМ using the same initial condition as in Khairoutdinov and Randall (2006), which is based on an idealization of LBA experiment in the Amazon. The model is initiated with a morning sounding (at 0730 LST) and forced only with prescribed surface fluxes as presented in Fig. 1.

Figure 2 shows the domain-averaged composite evolution of the ensemble-averaged cloud condensate and surface precipitation as a function of local time. The shallow cumulus clouds develop roughly at 9:50 in the morning, which is slightly later than the 3-D CSRМ results (see Fig. 1 in Khairoutdinov and Randall 2006). This may be due to the restriction of the 2-D dynamics in simulating the fine structure of shallow cumulus. On the other hand, the 2-D CSRМ captures an apparent transition from shallow to deep convection around 10:40 and the subsequent development of a deep convection phase in the last hour of simulation.

Because the growth of the shallow cumulus layer seems to increase more slowly than the deep cumulus, the simulations exhibit an apparent transition in the behavior of the convection. The ensemble-averaged evolution of the domain-averaged precipitation rate starts at about 11:00 in the morning and keeps increasing as the clouds grow deeper with values near  $18 \text{ mm day}^{-1}$  around 1:30 pm. This corresponds well with the 3-D CSRM results throughout the simulation. The growing variability of the precipitation rate is likely a sampling artifact; convective systems tend to organize into a few big cloud clusters in the deep convection stage. The development of precipitation and cloud condensate is not as smooth as in the 3-D CSRM results because even with the large ensemble, our simulation accesses many fewer degrees of freedom. In general, however, the benchmark ensemble shows sufficiently good agreement with the 3-D CSRM to warrant further study.

### *c. Sensitivity experiments*

In the benchmark simulation, we can imagine that various parameters could influence the transition. It is even conceivable that the transition is an artifact of some arbitrary feature of the initial data or forcing. If this is the case, it would be difficult to establish a useful concept of the transition. An idealized framework is therefore constructed for the sensitivity experiments. By reducing the parameter space, the key processes that control an apparent transition may be identified. We focus on the physical variables of the model. Sensitivities to other parameters, such as those that arise in the parameterization of turbulent and microphysical processes, are not considered, suffice to say they have been adjusted based on accumulated experience and understanding to produce the best possible simulation and

have not been tuned to increase the fidelity of these particular experiments.

The physical parameters introduced in these simulations include the initial profiles such as the temperature, moisture and horizontal wind, and diabatic tendencies associated with surface and radiative fluxes. The large-scale advective forcing of the temperature and moisture fields are set to zero. We also ignore the effects of the initial wind field by setting it to zero. The latter idealization is motivated by the data; weak winds are a typical feature in the Amazon soundings. The radiative heating of the atmosphere is also set to zero. Two factors motivate this choice: (i) The cloud fraction in this study is small and the effects of cloud-radiation interactions are beyond the scope of our interest. (ii) Our simulations are short so the long time effect of humidity-radiation feedbacks can be neglected. To identify whether or not the transition is an emergent property of the developing cumulus layer itself, as opposed to being forced at the surface, we fix the surface fluxes to be constant in time, at values equal to the time-averaged fluxes from the benchmark experiment. With this idealized surface forcing, the physical timing of the transition might be influenced, but (if it is an intrinsic feature of the developing convective layers) not its essential character. Such an approach is consistent with the past studies of the transition as they focus on the changing behavior of the internal dynamics or environmental profiles rather than the external forcing (e.g., Krueger et al. 1995b).

Under this idealized framework, the only remaining external parameters given to the model ensemble is the initial temperature and moisture data, and the random seeds. Figure 3 shows the lapse rate of potential temperature,  $\theta$ , and the relative humidity of the LBA soundings used by Khairoutdinov and Randall (2006). The finescale vertical structure in both profiles could conceivably influence the transition. For instance, the convective clouds can be

hampered by a sharp increase of stability or sharp decrease of moisture. To eliminate possible artifacts associated with the finescale structure of the initial profiles, we used smoothed profiles for the initial data. By doing so, we can also reduce the control variables to just two, one for stability and another for humidity, thereby helping isolate the relative role of these two quantities in regulating the buoyancy of clouds and convective transitions. The shape of the lapse rate of  $\theta$  indicates that the environment more or less follows the saturated adiabatic lapse rate. Therefore we can use the saturated adiabatic lapse rate to construct the control temperature parameter:  $\Gamma = M \cdot \Gamma_s + C$ , where  $\Gamma_s$  denotes the saturated lapse rate,  $M$  determines the shape of the lapse rate, and  $C$  determines the perturbation of initial stability. The shape parameter,  $M$ , is kept constant to 0.7 to match the Amazon sounding for all simulations. Following Guichard et al. (2004), the moisture profile is modeled with relative humidity rather than the mixing ratio. This assures no supersaturation for the experiments. The relative humidity profile of the LBA sounding is relatively uniform below 6 km and decreases with height above this level. Thus we set the relative humidity in the lower troposphere to a constant value and let it decrease linearly with height above 6 km (going to zero at 16 km). This roughly matches the observed humidity structure in the layer between 6-10 km. With the above simplification, we can focus our study on the influence of two control parameters, the perturbation of initial stability,  $C$ , and the relative humidity in the lower to middle troposphere. The humidity at the surface is not varied, as we did not wish cloud base to vary significantly across the simulations. The initial profiles of the lapse rate of potential temperature and relative humidity are presented in Fig. 3. Three different lapse rate profiles (marked as U, M, and S in which M (medium) is slightly more stable than U (unstable) and S (stable) is slightly more stable than M) with three relative humidity

profiles (marked as 80%, 85% and 90%) generate a set of 9 experiments as listed in Table 1. Remember that each experiment consists of an ensemble of 16 simulations whose results are averaged before analysis.

### 3. Temporal evolution

#### *a. Overview*

In analyzing these sensitivity experiments, we first evaluate whether the concept of a transition from shallow to deep convection is apparent in our idealization. We show that it is. This motivates a subsequent proposal whereby we define a transition time which we then attempt to model based on the various factors which influence it. The domain-averaged ensemble cloud condensate for all experiments is presented in Fig. 4. The results show a systematic dependence of the development of convection on the stability and the humidity. As one would expect, and in accord with previous work, the transition to deep convection happens earlier in moister and more unstable environments. This suggests that such idealization is a useful simplification of the problem. Take the experiment M85, for example, in which shallow cumulus clouds develop around  $t=1.5$  hr and grow in height roughly linearly in time (e.g., Stevens 2007). Around  $t=3.5$  hr, the convection does not deepen at the same rate anymore but instead accelerates.

The results also indicate the possibility of incorporating the effects of temperature and humidity into a single parameter. For example, the diagonal experiments (S90, M85, U80) look relatively similar to each other showing that the effects of stability can compensate the

humidity. Experiment M80 evolves similarly to S85, and U85 evolves similarly to M90. All in all, simulations across the array of experiments presented in Fig. 4 show qualitatively how the inhibition of a dry environment can compensate for additional CAPE associated with an environment characterized by a smaller lapse rate in potential temperature.

A deep convective regime is not evident in experiment S80, as by the end of simulation, the clouds have barely grown to the 4 km height. This is possibly a result of the time constraint of the simulation. Judging from other experiments, the development of a deep convective regime might happen later if we extend the experiments in time. In general, the results show that the transition of shallow to deep convection significantly responds to small variations of environmental lapse rate (less than  $0.2 \text{ K km}^{-1}$  below 10 km) and relative humidity (5%). From these results we conclude that the transition is a useful concept whose origin and timing merit explanation.

*b. The transition time*

In order to study the nature of the transition, it proves helpful to define it. For this purpose, we introduce the concept of the transition time which we define based on the changing rate of growth of the height of the center of cloud mass ( $Z_c$ ), defined as:

$$Z_c = \frac{\int \int q_c z \, dx dz}{\int \int q_c \, dx dz}, \quad (1)$$

where  $dx dz$  is an element of area,  $q_c$  is the mixing ratio of cloud condensate, and  $z$  is the vertical coordinate.  $Z_c$  is an integral quantity and tends to be a more robust measure than say precipitation rate or depth of the deepest clouds. The time evolution of  $Z_c$  for all experiments is presented in Fig. 5. During the period of shallow convection for each

set of experiments with the same stability,  $Z_c$  initially increases at roughly the same rate, followed by a pronounced rate of deepening as the layer transitions to the deep convective regime. Since the deep convection follows a different slope under different environmental conditions, it is clearer to define the transition based on the slope of shallow convection. A linear regression is fitted to the  $Z_c$  between 1 and 2 hour (called  $Z_{cr}$ ) and the transition time,  $t_*$ , is defined as the time when  $Z_c > 1.15Z_{cr}$ . Although the choice of 15% is subjective, changing criteria to 10% or 20% has little impact on the transition time in most cases.

The transition time of the sensitivity experiments is listed in Table 2. As discussed in the previous section, the values of  $t_*$  for the diagonal experiments (S90, M85, U80) are very close to each other, with U85 and M90 having the same  $t_*$  suggesting that the transition time can capture the changing behavior of the time evolution of convection. Thus, we can use this index to further explore the control mechanism of the transition.

## 4. What controls the transition?

### *a. Previous studies*

Previous work suggests that a number of factors may be important to the transition time. Before introducing any new ideas, we first explore the dependence of the transition time on the environmental moisture and stability and the effects of cold pools and convective inhibition (CIN) of the air parcels. Figure 6 shows how  $t_*$  varies with critical moisture and stability. The critical moisture is defined as the relative humidity in the free troposphere (3 km) at  $t_*$  and the critical stability is defined as the CAPE (convective available potential

energy) at  $t_*$ . The results support the idea that a moister free troposphere favors deep convection and leads to an earlier transition, as shown by Derbyshire et al. (2004). That said, the environmental lapse rate of potential temperature also significantly affects  $t_*$ , this point of course being taken for granted in earlier work. Consequently, larger CAPE suggests the possibility for early development of deep convection, but the variation of  $t_*$  among different relative humidity is large. For many parameterizations incorporated in large-scale models (as embodied in SCMs), deep convection develops with the initial appearance of CAPE which almost always occurs much too soon.

Attempts to relate  $t_*$  to a cold pool index proved unsuccessful. To show this, we present the time evolution of cloud width near the cloud base from the M-class experiments in Fig. 7a. The results suggest that during transition, the difference of cloud size among experiments is small, although the mechanism for producing larger clouds through the development of cold pools becomes evident after the transition time (roughly at  $t=4-6$  hr). This indicates that at least in these cases there are other mechanisms that contribute to the transition prior to the cold pool/precipitation interactions, but that the development of cold pools may constitute an important feedback in the subsequent development of convection.

The CIN for the air parcels is usually considered as an important factor for inhibiting development of deep convection. The time evolution of CIN is presented in Fig. 7b. The results show that with the deepening subcloud mixed layer, the CIN decreases rapidly in the first hour. The minimum CIN occurs roughly during the onset of shallow cumulus clouds at  $t = 1.5$  hr. The difference among experiments is very small. In addition, the CIN is practically zero for all experiments during the transition. Hence it was not apparent to us how to usefully incorporate this information in a way that improves the prediction of, say,

CAPE based estimates of the transition time.

*b. The cloud-layer instability argument*

The above experiments suggest that the previous lines of arguments (cold pool and CIN) do not, on their own, provide an adequate explanation of the transition time between shallow and deep convection, nor were they intended to. After exploring a variety of ideas, we found that the transition time can be rationalized using parcel theory but not as is traditionally done based on non- (or weakly) entraining parcels which set the depth of the convective layer (perhaps subject to some maximum value of CIN). Depending on the details of how one constitutes test parcels, the clouds can behave rather differently. This motivates us to look into the ensemble behavior of cloud trajectories leading up to and through the time of the transition.

Figure 8 presents a closer look of the mean virtual potential temperature profile,  $\theta_v$ , in the lower troposphere. The dotted line represents the averaged cloud properties defined by averaging all the cloudy points ( $q_c > 0$ ) irrespective of their buoyancy. This analysis shows that while the simulated cloud base height is roughly the same as that expected from the adiabatic expansion of undiluted parcels, its thermodynamic state evolves much differently. The averaged shallow clouds follow a thermodynamic trajectory that is always colder than the environment, reflecting the fact that they are actively entraining. And so while an undiluted, or weakly entraining parcel may be unstable, the clouds are *on average* stable relative to their environment. These clouds do not, on average, access any CAPE.

A conserved variable diagram is a useful tool to look at the overall behavior of the

clouds (e.g., Neggers et al. 2002). In our analysis, the liquid water potential temperature,  $\theta_l$ , is plotted versus the total mixing ratio,  $q_t$ , (water vapor plus cloud liquid water). These thermodynamic variables are conserved under isentropic changes of phase, hence they can only change by diabatic processes such as mixing, precipitation or radiation. Given that radiation and precipitation processes are not significant in the shallow phase, such a diagram usually characterizes the mixing processes of the clouds and the environment. Figure 9 is an example of such a diagram for experiment M85 for  $t=2.5$  hr and  $t=3.5$  hr at 1500 m. The vertical profile of the horizontal mean values in the lower levels is also plotted with open circles. The saturation curve and zero buoyancy line of this level ( $z=1500$  m) are fundamental lines given a specification of pressure, and help divide the figure into four sectors. All points above the saturation line represent the clouds (dots, light grey), and the points to the right of the zero buoyancy line represent buoyant cloud cores (squares, dark grey).

The cloudy points in the diagram have a broad distribution showing the effects of entrainment. Note that an undiluted parcel released from the surface will not change its position on the diagram since both  $\theta_l$  and  $q_t$  are conserved. The black dot in the diagram represents the average properties of the clouds. At  $t=2.5$  hr, the average cloud at this level is not buoyant (although an undiluted parcel lifted from the surface is very buoyant) while at  $t=3.5$  hr, after the transition, the average cloud becomes buoyant. If the relation between the clouds and the environment is similar at different levels, as shown in Fig. 8, the stability of the shallow cumulus layer can be represented through the consideration of the lapse rate changes of both the environment and the clouds.

Thus, our hypothesis of the transition from shallow to deep convection is that: shallow

convection persists until the environment of the shallow cumulus layer becomes unstable to the *average* cloud properties. Figure 10 presents a schematic illustration of this evolution. The thick solid and dash lines represent the time evolution of  $\theta_v$  for the environment and clouds. Throughout the transition, the averaged cloud lapse rate of  $\theta_v$  increases while the environmental lapse rate of  $\theta_v$  decreases. Hence, as measured by the properties of the *average* cloud, the layer is becoming destabilized. Eventually, the lapse rate of  $\theta_v$  of the clouds becomes larger than the environment at which the vertical development of clouds will eventually cause them to become buoyant, thus favoring further development, hence deep convection. The change of the environmental profile is due to the preconditioning effects of the shallow cumulus through the evaporative cooling of cloud condensate. These effects tend to destabilize the layer resulting in a decrease of the environment lapse rate through the period leading up to the transition time. Changes in the lapse rate of the average cloud may also reflect the changing of environment, as they result less from the changing distribution of mixtures (along a mixing line) and more from changes in the end states of the conserved variable diagram. Since the environment becomes moister and more unstable, the mixing between the clouds and the environment becomes less effective in diluting and stabilizing the clouds.

To confirm this idea, we diagnose the lapse rate of  $\theta_v$  for both the average cloud and the environment in the shallow cumulus layer from our simulations. To better quantify the effects of the shallow cumulus, the layer base is defined as the layer of maximum cloud fraction. This is located near cloud base where cloud fractions are typically around 20%. The top of the shallow cumulus layer is defined as the first layer below 2.4 km and above cloud base where the cloud fraction falls below 2%. If cloud fraction does not fall below

this threshold below 2.4 km, we cap the layer at 2.4 km. With this definition of the shallow cumulus layer, we can diagnose the time evolution of the lapse rate for the clouds and the environment. Figure 11 presents the time evolution of the vertical profile of the lapse rate of  $\theta_v$  for experiment M85. The environment lapse rate is around zero near the surface and increases to the value of its initial condition with increasing height. At  $t=2$  hr, the average cloud lapse rate is smaller than the environment suggesting that the clouds are on average not buoyant. With the increase of time, the lapse rate of the environment becomes smaller and the lapse rate near the cloud base become larger although the former (preconditioning effect) dominates. About 2/3 of the shallow cumulus becomes buoyant to the environment at  $t=4$  hr. The  $t_*$  for this experiment is about 3.5 hours. We can see that the lapse rates of the environment and clouds do cross around the transition.

To better quantify  $t_*$ , the lapse rates of the clouds and the environment are estimated as the best fit (in a least-squares sense) line to the data in the shallow cumulus layer of the clouds ( $\Gamma_{cld}$ ) and the environment ( $\Gamma_{env}$ ). In this case, when  $\Gamma_{cld} > \Gamma_{env}$ , we can say that the average clouds can become buoyant. The time evolution of  $\Gamma_{env}$  shows that the environment is continuously destabilized by the shallow cumulus clouds while the regressed lapse rate of the clouds slightly (albeit less robustly) increases throughout the simulation. Around  $t=3.5$  hr, the regressed lapse rate of the clouds is larger than the environment. We call the time when the two lapse rates cross the "crossing time" of transition. For all 9 experiments, the crossing time is defined with the same method. To test our hypothesis that the transition occurs when the shallow clouds become buoyant, a scatter plot of the transition time versus the crossing time is presented in Fig. 12. In the more unstable and moister experiments, the crossing time tends to be a bit later than the transition time while for the drier cases, the

crossing time tends to be a bit earlier than the transition time. So while there is room for improvement we believe that this definition of the crossing time adequately encapsulates the combined effects of humidity and temperature on regulating the transition between shallow and deep convection.

*c. The mixing model*

With the cloud layer instability argument in mind, it is interesting to see if we can develop a simple model that describes the changes of lapse rate in both the environment and clouds because such a model would be useful for improving convection parameterizations. In Fig. 9, we can see that the cloudy points roughly distribute themselves along a line connecting the mean state of the surface and the observed level. This demonstrates that the distributions of the conserved variables of the cloud ensemble are highly correlated and indicates that the mixing processes in the cumulus ensemble might admit a geometric interpretation. If we assume that the clouds consist of a uniformly distributed mixing fraction of air between the surface and the observed level, the mean properties of the clouds should be half way in between the surface and the saturation curve on the line connecting the surface and the observed level. A tick mark is plotted on the diagram to show this point. The assumption is probably too simple of a representation of the entrainment source of the clouds. But our main focus here is to see if this mixing model can represent the stability of the mean clouds. Overall the mean cloud properties, and the average properties of uniformly distributed mixtures are relatively similar. This suggests that the change of cloud lapse rate can be parameterized by the change of the environment only.

The profile of this geometric mixing model can be constructed by assuming that the mean cloud parcel at any given level consists of mixtures of near surface air and air with the mean properties at that level. Following the same procedure, we can diagnose the time evolution of the lapse rate of  $\theta_v$  of the mixing model as shown in Fig. 13. We can see that the qualitative behavior of the mixing model captures the state of the simulated clouds reasonably well. The time evolution of the lapse rate of the mixing model shows a more systematic increase in responding to the change of the environment. Therefore, a crossing time of the mixing model can also be determined using the same methodology as before. A scatter plot of the crossing time of the mixing model versus the transition time is presented in Fig. 14. The results suggest that the mixing model can be used to estimate the transition time. The results also suggest that the change of cloud lapse rate of can be represented if the change of the environment is known.

Our simple model helps to explain how the clouds respond to the change of the environment. The evolution of the environmental lapse rate, however, is also strongly modified by the shallow cumulus clouds. The next step is to better understand how the representation of shallow convection affects this evolution.

## 5. Summary and discussion

In this study, a 2-D CSRМ (Cloud-System Resolving Model) is used to assess the control mechanism for the transition from shallow to deep convection. By comparing with the 3-D CSRМ under conditions taken from the Large-scale Biosphere Atmosphere (in the Amazon) field study, we show that the 2-D CSRМ represents the main features evident in previous

3-D simulations reasonably well.

To extract the essence of the transition from shallow to deep convection, we use an idealized framework to highlight the role of two control parameters, the free tropospheric lapse rate of potential temperature and the relative humidity. The systematic dependence of the development of convection on the potential temperature lapse rate and the humidity show that the concept of a convective transition is a meaningful one. A transition time can be defined to evaluate the relationship of the transition time to the evolution of the thermodynamic state of the different simulations.

The results show that the transition time depends on both the moisture and the potential temperature lapse rate, but in a way that previous ideas do not fully encapsulate, notwithstanding that aspects of our arguments are at least qualitatively anticipated by Houston and Niyogi (2007). We hypothesize that shallow convection persists until the environment of the shallow cumulus layer becomes unstable to the average cloud properties. This permits the transition time to be predicted given a consideration of the stability of the shallow cumulus layer. By analyzing the time evolution of the lapse rate of virtual potential temperature of the environment and that of the clouds in the shallow cumulus layer, we show that the transition coincides with the time when the lapse rate of the clouds becomes larger than that of the environment, suggesting that transition happens when shallow clouds become, on average, buoyant.

We construct a simple model which shows that the mean cloud properties can be usefully related to the mean environmental profiles. The geometric mixing model which assumes that the clouds consist of a uniformly distributed mixing fraction of air between the surface and the observed level in the Paluch diagram is used to represent the mean cloud properties. The

overall behavior of the simple mixing model suggests that the time evolution of the cloud lapse rate in the shallow cumulus layer can be represented given knowledge of the surface and environmental properties. The results also suggest the importance of the shallow cumulus in preconditioning the environment for the development of the deep convection. While our experiments are constructed under conditions over the Amazon, the ideas we invoke are general and may be applicable to other circumstances (i.e. over the ocean or over drier land). Those ideas are readily testable with data. Thus, in addition to developing our understanding of how the representation of shallow convection affects the environmental stability, future work should focus on evaluating the extent to which processes we articulate here may be relevant to the diurnal evolution of clouds.

*Acknowledgments.*

The authors thank two anonymous reviewers for their helpful comments and suggestions, which greatly improved the presentation of our ideas. This research is supported by the NSU grant ATM 0425247 (CMMAP) through CSU contract G-3045-1 to UCLA and DOE Cooperative Agreement DE-FG02-06ER64302 through CSU contract G-3818-1 to UCLA.

## REFERENCES

- André, J. C., G. De Moor, P. Lacarrere, and R. Du Vachat, 1976: Turbulence approximation for inhomogeneous flows: Part I. the clipping approximation. *J. Atmos. Sci.*, **33**, 476–481.
- André, J. C., G. De Moor, P. Lacarrere, and R. Du Vachat, 1978: Modeling the 24-hour evolution of the mean and turbulent structures of the planetary boundary layer. *J. Atmos. Sci.*, **35**, 1861–1883.
- Bechtold, P., J.-P. Chaboureau, A. Beljaars, A. Betts, M. Kohler, M. Miller, and J.-L. Redelsperger, 2004: The simulation of the diurnal cycle of convective precipitation over land in a global model. *Quart. J. Roy. Met. Soc.*, **139**, 3119–3137.
- Betts, A. and C. Jakob, 2002: Study of diurnal cycle of convective precipitation over amazonia using a single column model. *J. Geophys. Res.*, **107**, 4732, doi:10.1029/2002JD002264.
- Chaboureau, J.-P., F. Guichard, J.-L. Redelsperger, and J.-P. Lafore, 2004: The role of stability and moisture in the diurnal cycle of convection over land. *Quart. J. Roy. Met. Soc.*, **130**, 3105–3117.
- Chen, J.-M., 1991: Turbulence-scale condensation parameterization. *J. Atmos. Sci.*, **48**, 1510–1512.
- Derbyshire, S. H., I. Beau, P. Bechtold, J.-Y. Grandpeix, J.-M. Piriou, J.-L. Redelsperger, and P. M. M. Soares, 2004: Sensitivity of moist convection to environmental humidity. *Quart. J. Roy. Met. Soc.*, **130**, 3055–3080.

- Fu, Q., S. K. Krueger, and K. N. Liou, 1995: Interactions of radiation and convection in simulated tropical cloud clusters. *J. Atmos. Sci.*, **52**, 1310–1328.
- Guichard, F., et al., 2004: Modeling the diurnal cycle of deep precipitating convection over land with cloud-resolving models and single-column models. *Quart. J. Roy. Met. Soc.*, **130**, 3139–3972.
- Houston, A. L. and D. Niyogi, 2007: The sensitivity of convective initiation to the lapse rate of the active cloud-bearing layer. *Mon. Wea. Rev.*, **135**, 3013–3032.
- Johnson, R. H. and B. E. Mapes, 2001: Mesoscale processes and severe convective weather. *Severe Convective Storms, Meteor. Monogr.*, No. 50, Amer. Meteor. Soc., 71–122.
- Khairoutdinov, M. and D. A. Randall, 2006: High-resolution simulation of shallow-to-deep convection transition over land. *J. Atmos. Sci.*, **63**, 3421–3436.
- Krueger, S. K., 1988: Numerical simulation of tropical cumulus clouds and their interaction with the subcloud layer. *J. Atmos. Sci.*, **45**, 2221–2250.
- Krueger, S. K. and A. Bergeron, 1994: Modeling the trade cumulus boundary layer. *Atmos. Res.*, **33**, 169–192.
- Krueger, S. K., Q. Fu, K.-N. Liou, and H.-N. Chin, 1995a: Improvements of an ice-phase microphysics parameterization for use in numerical simulations of tropical convection. *J. Appl. Meteor.*, **34**, 281–287.
- Krueger, S. K., G. T. McLean, and Q. Fu, 1995b: Numerical simulation of the stratus-

- to-cumulus transition in the subtropical marine boundary layer. Part I: Boundary-layer structure. *J. Atmos. Sci.*, **52**, 2839–2850.
- Kuang, Z. and C. Bretherton, 2006: A mass-flux scheme view of a high-resolution simulation of a transition from shallow to deep cumulus convection. *J. Atmos. Sci.*, **63**, 1895–1909.
- Lin, C. and A. Arakawa, 1997: The macroscopic entrainment processes of simulated cumulus ensemble. Part I: Entrainment sources. *J. Atmos. Sci.*, **54**, 1027–1043.
- Lin, Y. L., R. D. Farley, and H. D. Orville, 1983: Bulk parameterization of the snow field in a cloud model. *J. Climate Appl. Meteor.*, **22**, 1065–1092.
- Liou, K.-N., Q. Fu, and T. P. Ackerman, 1988: A simple formulation of the delta-four-stream approximation for radiative transfer parameterizations. *J. Atmos. Sci.*, **45**, 1940–1948.
- Lord, S. J., H. E. Willoughby, and J. M. Piotrowicz, 1984: Role of a parameterized ice-phase microphysics in an axisymmetric, non-hydrostatic tropical cyclone model. *J. Atmos. Sci.*, **41**, 2836–2848.
- Moeng, C.-H., et al., 1996: Simulation of a stratocumulus-topped planetary boundary layer: Intercomparison among different numerical codes. *Bull. Amer. Meteor. Soc.*, **77**, 261–278.
- Neggers, R. A. J., A. P. Siebesma, and H. J. J. Jonker, 2002: A multiparcel model for shallow cumulus convection. *J. Atmos. Sci.*, **59**, 1655–1668.
- Redelsperger, J. L., et al., 2000: A GCSS model intercomparison for a tropical squall line observed during toga-coare. Part I: Cloud-resolving models. *Quart. J. Roy. Met. Soc.*, **126**, 823–863.

- Stevens, B., 2007: On the growth of layers of nonprecipitating cumulus convection. *J. Atmos. Sci.*, **64**, 2916–2931.
- Tao, W.-K., S. Lang, J. Simpson, C.-H. Sui, B. Ferrier, and M.-D. Chou, 1996: Mechanisms of cloud-radiation interaction in the tropics and midlatitudes. *J. Atmos. Sci.*, **53**, 2624–2651.
- Xu, K.-M., A. Arakawa, and S. K. Krueger, 1992: The macroscopic behavior of cumulus ensembles simulated by a cumulus ensemble model. *J. Atmos. Sci.*, **49**, 2402–2420.
- Xu, K.-M. and S. K. Krueger, 1991: Evaluation of cloudiness parameterizations using a cumulus ensemble model. *Mon. Wea. Rev.*, **119**, 342–367.
- Xu, K.-M. and D. A. Randall, 1996: Explicit simulation of cumulus ensembles with the GATE Phase III data: Comparison with observations. *J. Atmos. Sci.*, **53**, 3710–3736.
- Ziegler, C. L., T. J. Lee, and R. A. Pielke, 1997: Convective initiation at the dryline: A modeling study. *Mon. Wea. Rev.*, **125**, 1001–1026.
- Ziegler, C. L. and E. N. Rasmussen, 1998: The initiation of moist convection at the dryline: Forecasting issues from a case study perspective. *Wea. Forecasting*, **13**, 1106–1131.

# List of Figures

1	The initial condition for the benchmark simulation, a morning sounding over the Amazon region with prescribed surface fluxes. Here the solid and dashed lines in the surface fluxes represent latent heat flux and sensible heat flux, respectively. . . . .	30
2	The domain averaged and ensemble cloud condensate with contour interval $0.01 \text{ g kg}^{-1}$ and surface precipitation for the benchmark simulation. The error bar in surface precipitation represents the standard deviation of the 16 realizations. . . . .	31
3	The initial thermodynamic profiles for the Amazon sounding and the idealized experiments. The figure on the left presents the environmental stability ( $\Gamma$ ) which is defined as $d\theta/dz$ . The figure on the right presents the environmental relative humidity. See text for more details. . . . .	32
4	The domain averaged and ensemble averaged mixing ratio of cloud condensate for all experiments. The contour interval is $0.01 \text{ g kg}^{-1}$ . . . . .	33
5	The center of cloud mass ( $Z_c$ ) for all experiments. The thin solid line represents a linear regression fitted to $Z_c$ between 1 and 2 hour (called $Z_{cr}$ ) and the shading indicates the area between $1.1$ - $1.2 Z_{cr}$ . . . . .	34

6	<p>The scatter plots of the transition time versus critical moisture (relative humidity) and stability (CAPE). Variations of <math>t_*</math> between 1.1-1.2 <math>Z_{cr}</math> are shown as horizontal lines around <math>t_*</math>. The CAPE/CIN used in this study is calculated by the sum of the positive/negative area when following a parcel pseudo-adiabatically to its neutral buoyancy level. The initial parcel thermodynamic properties are defined by giving parcels the average thermodynamic properties of the lower 500 m. . . . .</p>	35
7	<p>The ensemble averaged time evolution of (a) the cloud width at the cloud base and (b) convective inhibition (CIN) for the M-class experiments. The cloud base is defined as the height of the maximum cloud fraction near the surface. The transition time is marked in the figure. . . . .</p>	36
8	<p>Ensemble averaged mean profiles of <math>\theta_v</math> at 2 hours for experiment M85. <math>\theta_v</math> is defined as <math>\theta_v = \theta(1 + 0.61q_v - q_c)</math> where <math>q_v</math> and <math>q_c</math> represents the mixing ratio of water vapor and cloud condensate. See text for more detail. . . . .</p>	37
9	<p>The scatter plot of total water mixing ratio (<math>q_t</math>) and the liquid water potential temperature (<math>\theta_l</math>) of the cloudy points for experiment M85 before and after transition. The dotted line represents the line connecting the surface point and the observation level. The tick mark and the large dot represent the mean properties of the mixing model and the clouds. . . . .</p>	38

10	A schematic illustration of transition from shallow to deep convection. The thick solid and dash lines represents the environment and cloud $\theta_v$ , respectively. The environment $\theta_v$ is averaged over the entire domain while the cloud $\theta_v$ is averaged over cloudy points only. The three sets of profiles represent the profiles before, during and after the transition. See text for more detail. . . .	39
11	The vertical profiles of the lapse rate of $\theta_v$ in the shallow cumulus layer and the time evolution of the regressed lapse rate of $\theta_v$ for experiment M85. The solid and dash lines represent the environment and the clouds, respectively.	40
12	Same as in Fig. 6 except for the transition time versus crossing time. . . . .	41
13	As in Fig. 11 except for the mixing model. . . . .	42
14	As in Fig. 6 except for the transition time versus crossing time of mixing model.	43

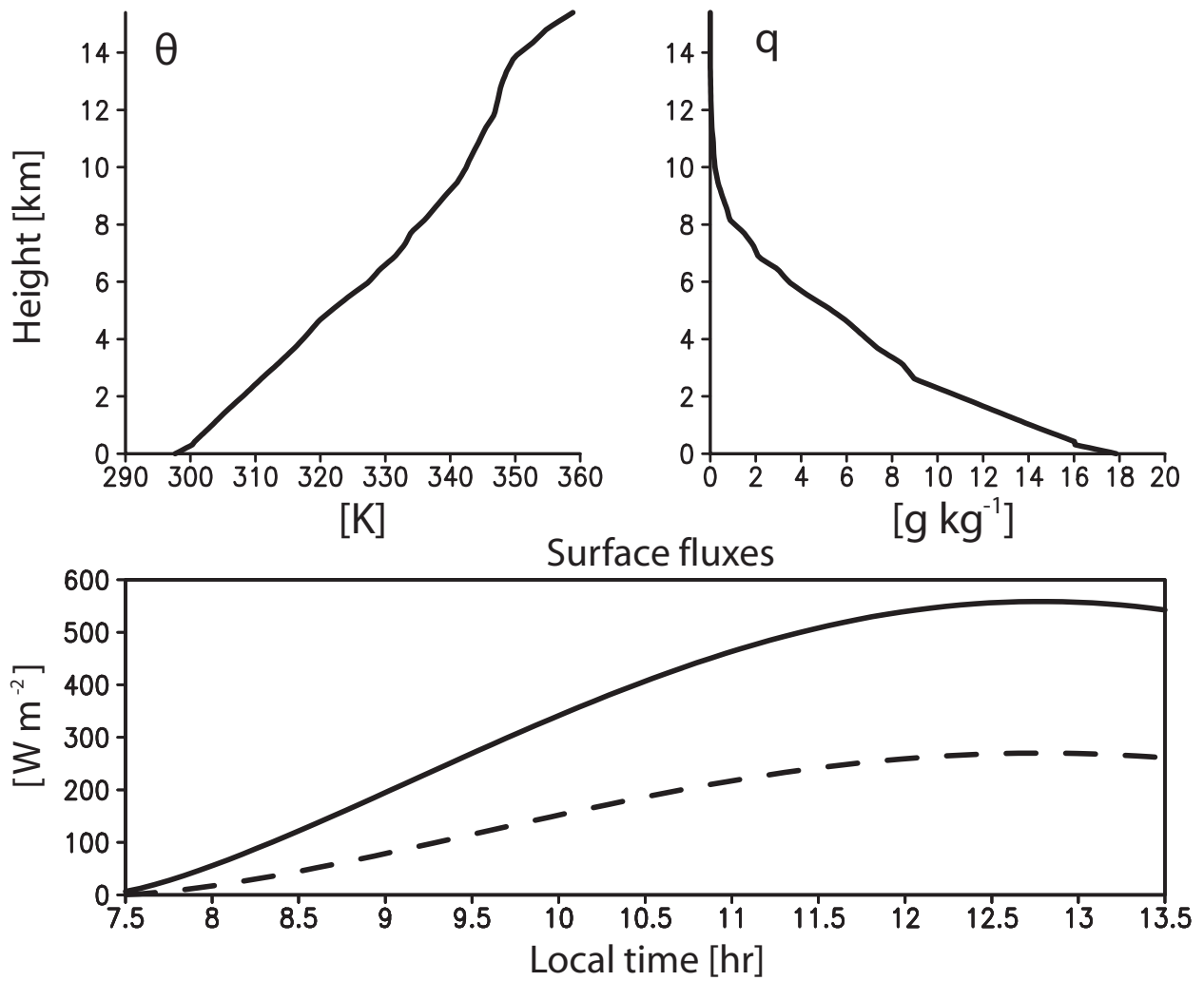


FIG. 1. The initial condition for the benchmark simulation, a morning sounding over the Amazon region with prescribed surface fluxes. Here the solid and dashed lines in the surface fluxes represent latent heat flux and sensible heat flux, respectively.

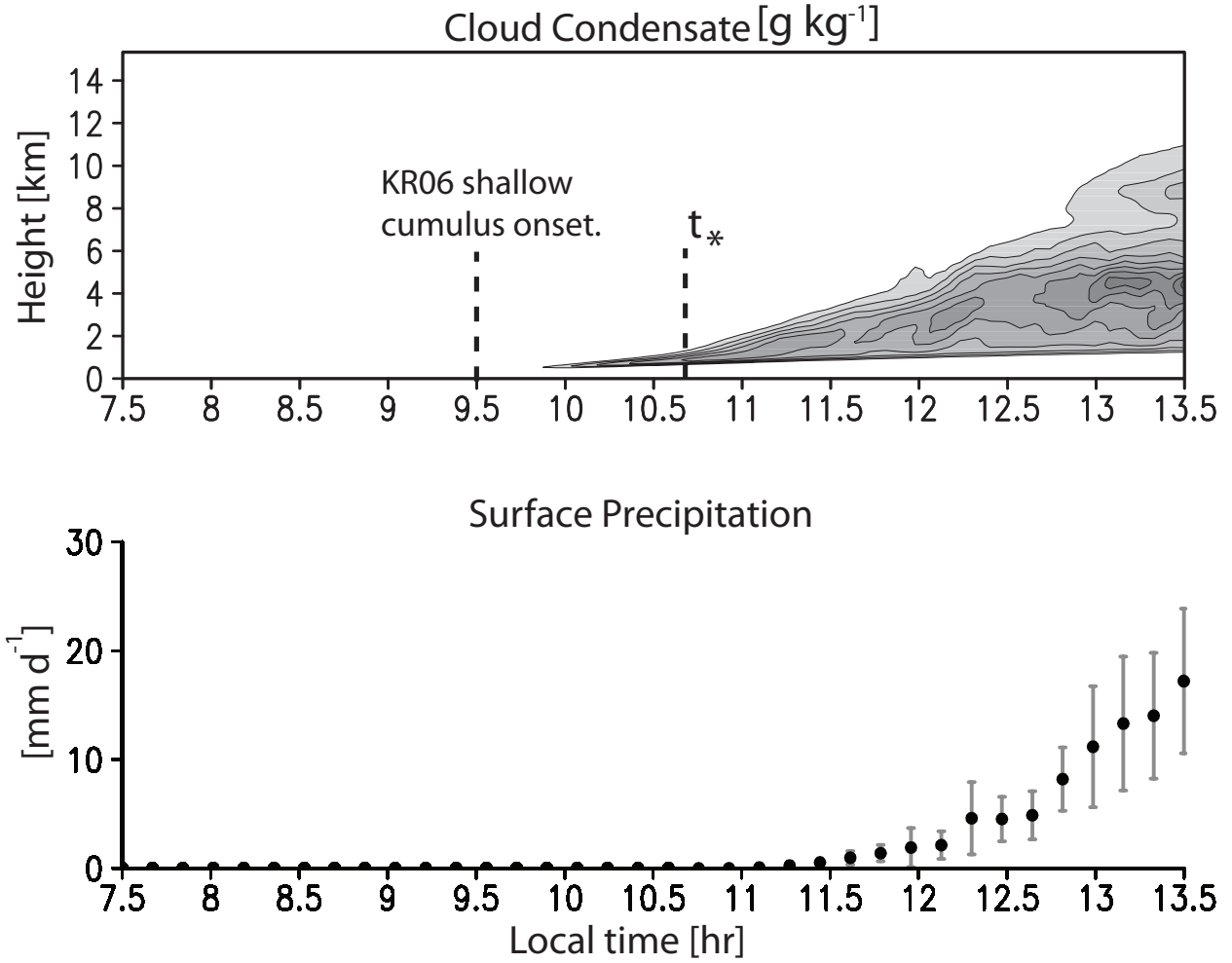


FIG. 2. The domain averaged and ensemble cloud condensate with contour interval  $0.01 \text{ g kg}^{-1}$  and surface precipitation for the benchmark simulation. The error bar in surface precipitation represents the standard deviation of the 16 realizations.

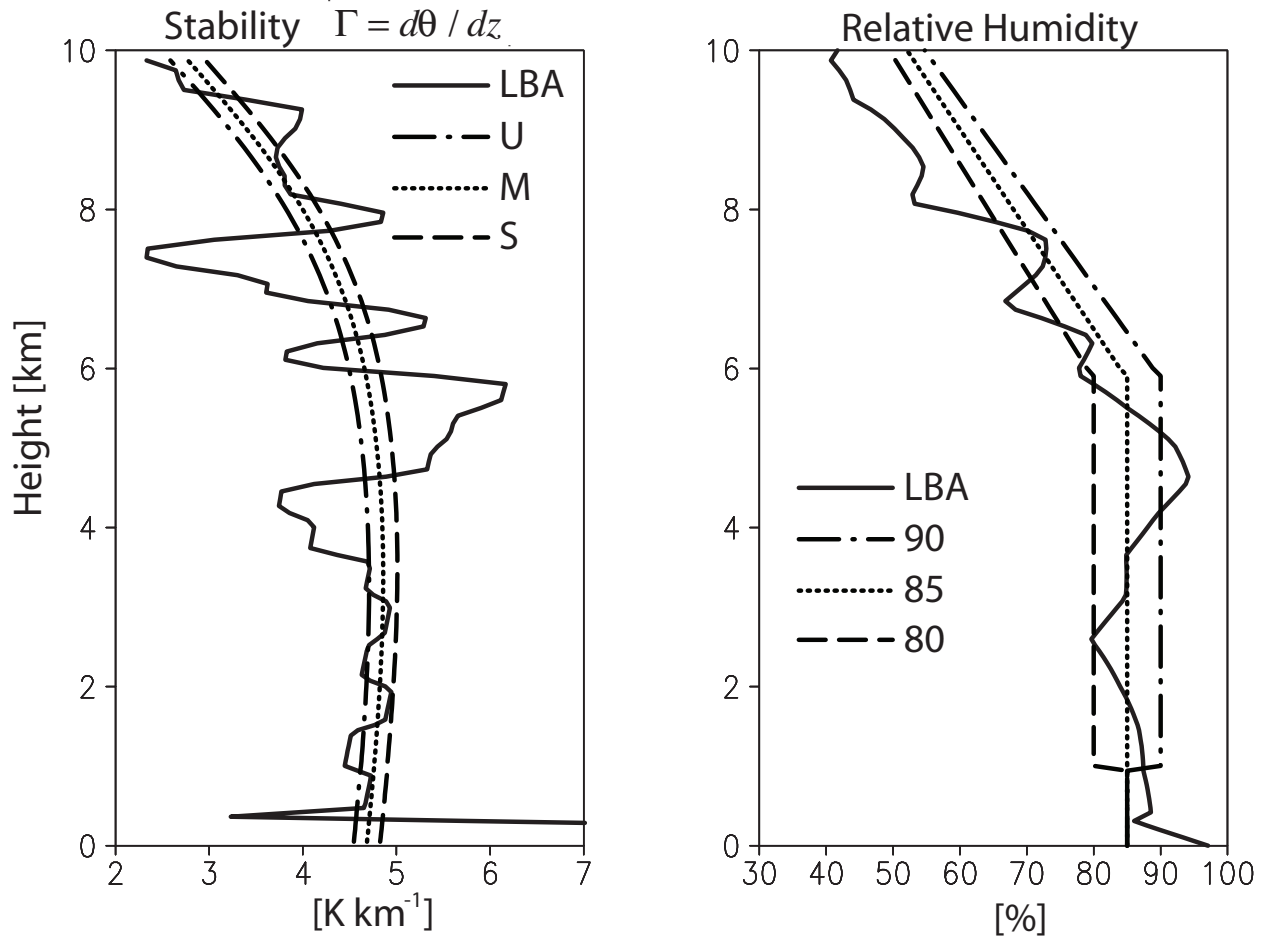


FIG. 3. The initial thermodynamic profiles for the Amazon sounding and the idealized experiments. The figure on the left presents the environmental stability ( $\Gamma$ ) which is defined as  $d\theta/dz$ . The figure on the right presents the environmental relative humidity. See text for more details.

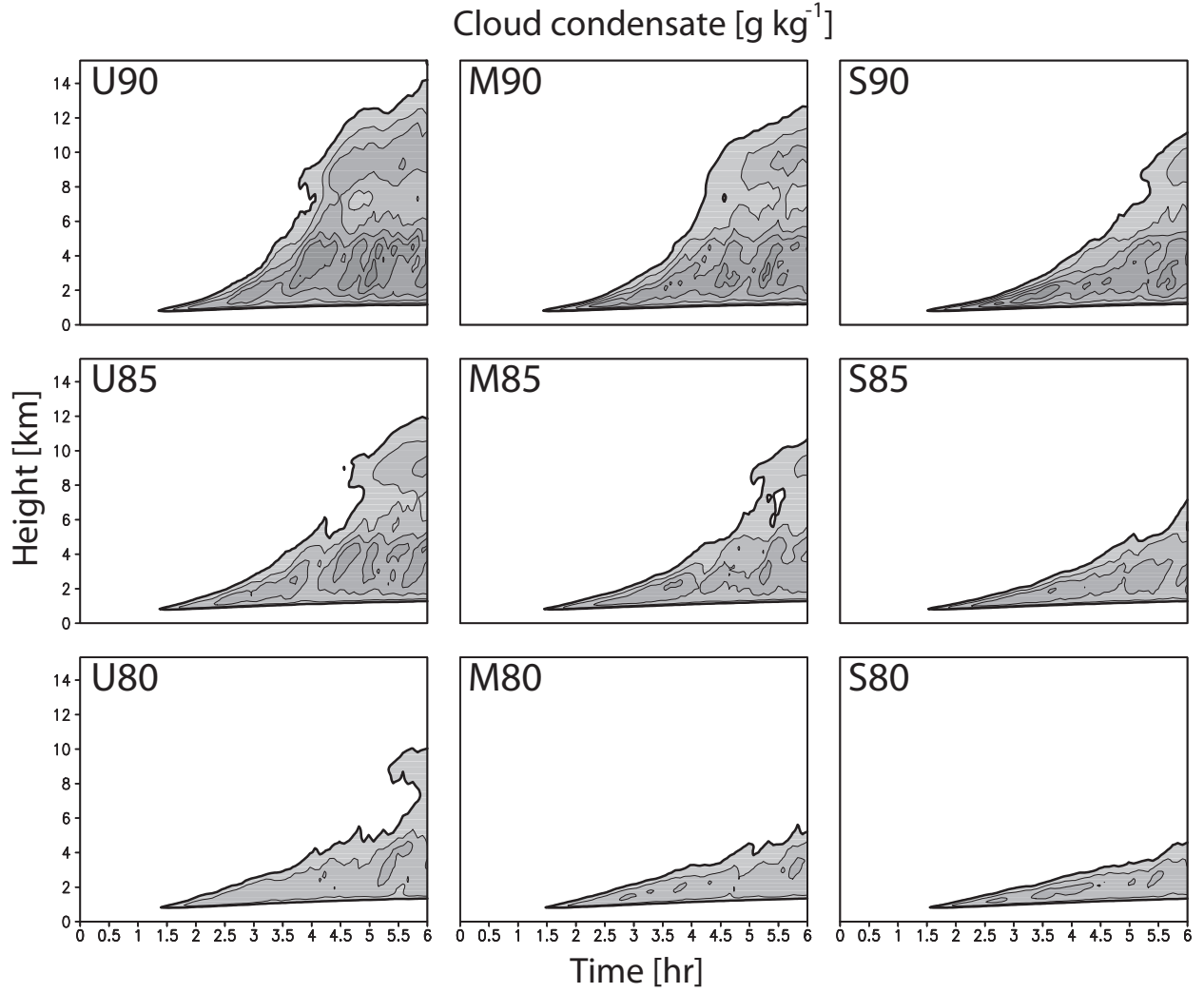


FIG. 4. The domain averaged and ensemble averaged mixing ratio of cloud condensate for all experiments. The contour interval is  $0.01 \text{ g kg}^{-1}$ .

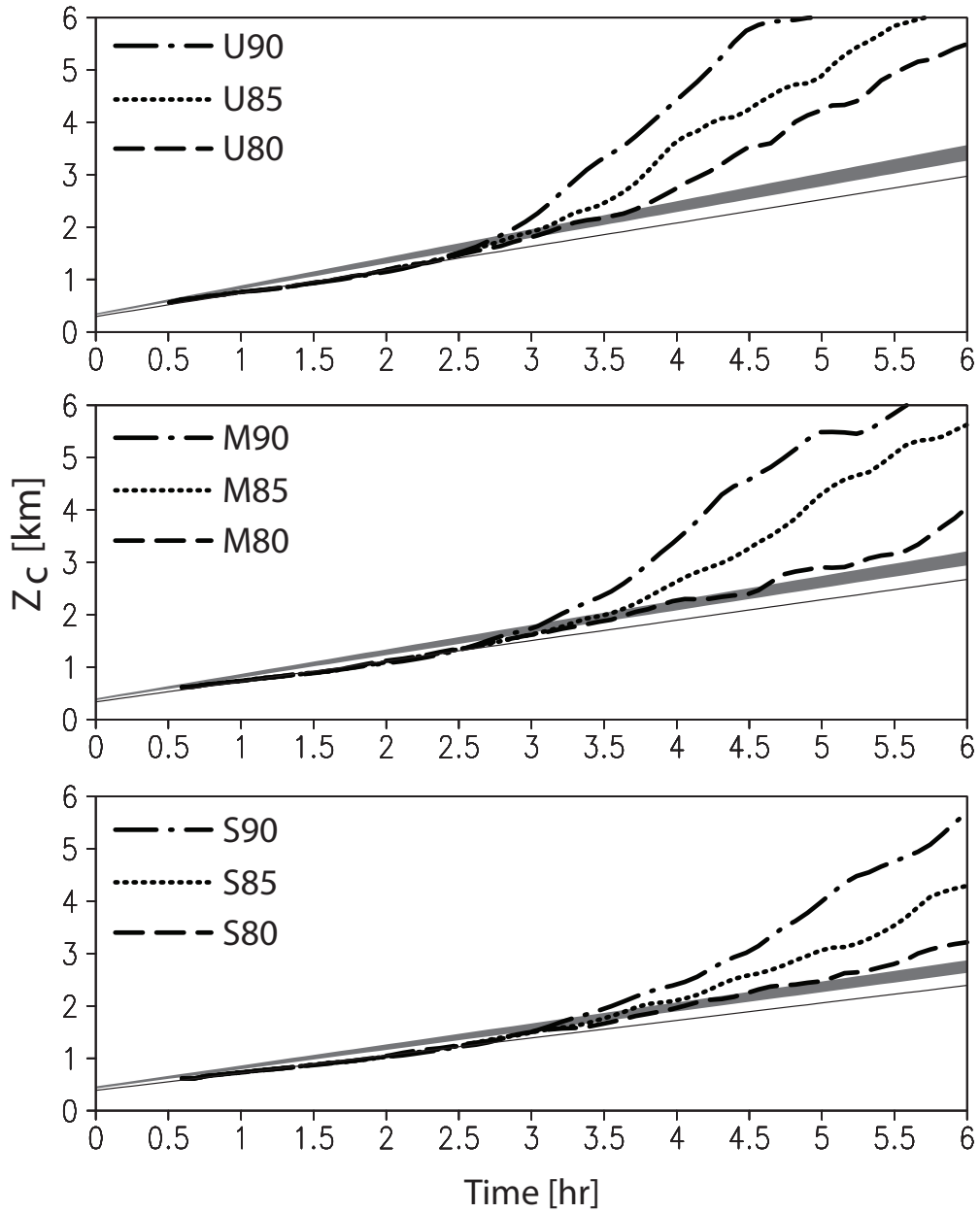


FIG. 5. The center of cloud mass ( $Z_c$ ) for all experiments. The thin solid line represents a linear regression fitted to  $Z_c$  between 1 and 2 hour (called  $Z_{cr}$ ) and the shading indicates the area between  $1.1$ - $1.2$   $Z_{cr}$ .

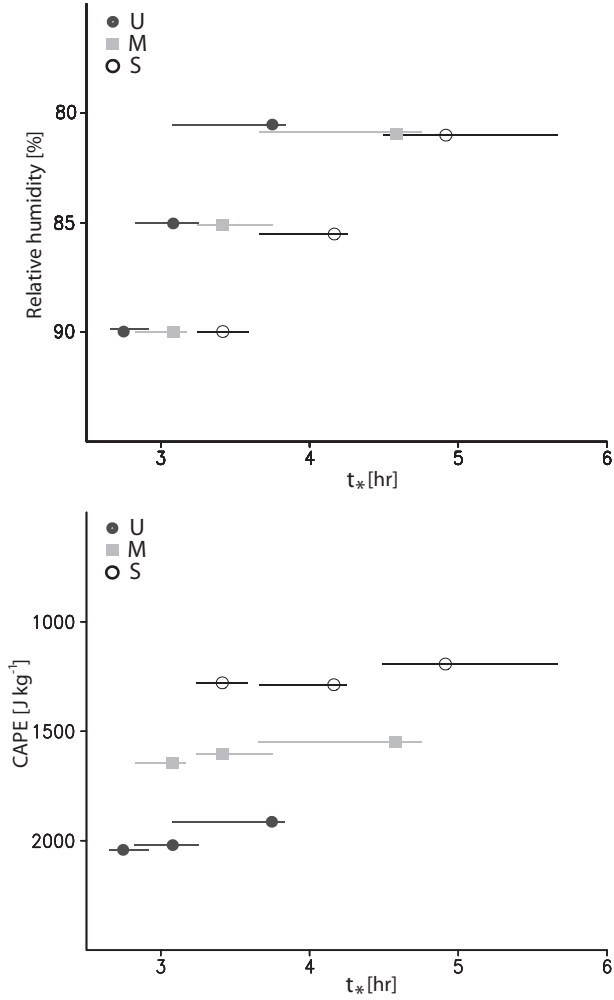


FIG. 6. The scatter plots of the transition time versus critical moisture (relative humidity) and stability (CAPE). Variations of  $t_*$  between 1.1-1.2  $Z_{cr}$  are shown as horizontal lines around  $t_*$ . The CAPE/CIN used in this study is calculated by the sum of the positive/negative area when following a parcel pseudoadiabatically to its neutral buoyancy level. The initial parcel thermodynamic properties are defined by giving parcels the average thermodynamic properties of the lower 500 m.

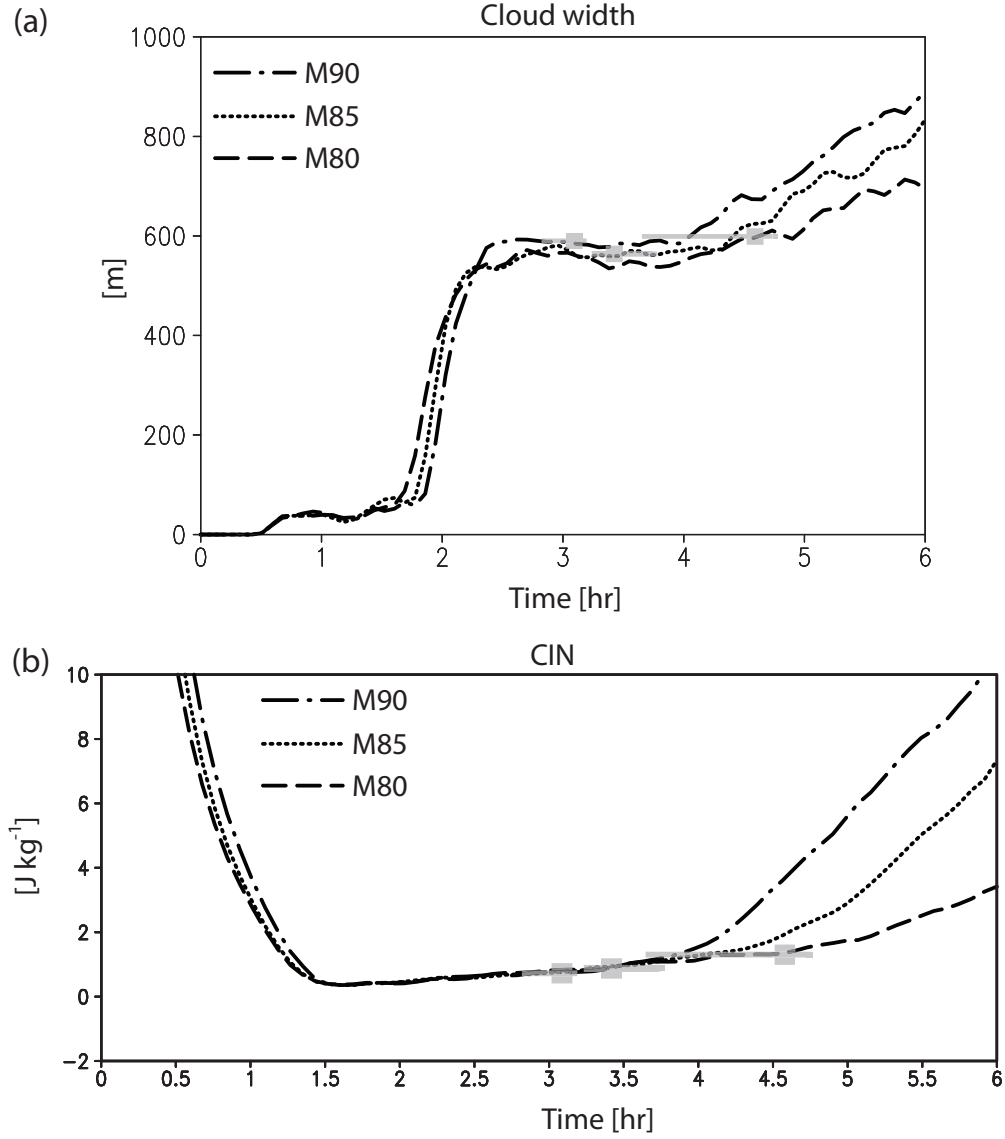


FIG. 7. The ensemble averaged time evolution of (a) the cloud width at the cloud base and (b) convective inhibition (CIN) for the M-class experiments. The cloud base is defined as the height of the maximum cloud fraction near the surface. The transition time is marked in the figure.

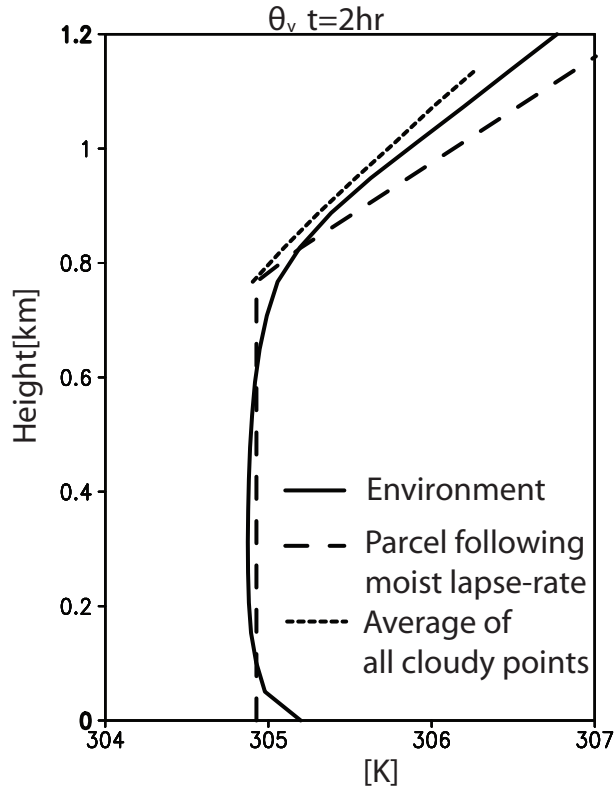


FIG. 8. Ensemble averaged mean profiles of  $\theta_v$  at 2 hours for experiment M85.  $\theta_v$  is defined as  $\theta_v = \theta(1 + 0.61q_v - q_c)$  where  $q_v$  and  $q_c$  represents the mixing ratio of water vapor and cloud condensate. See text for more detail.

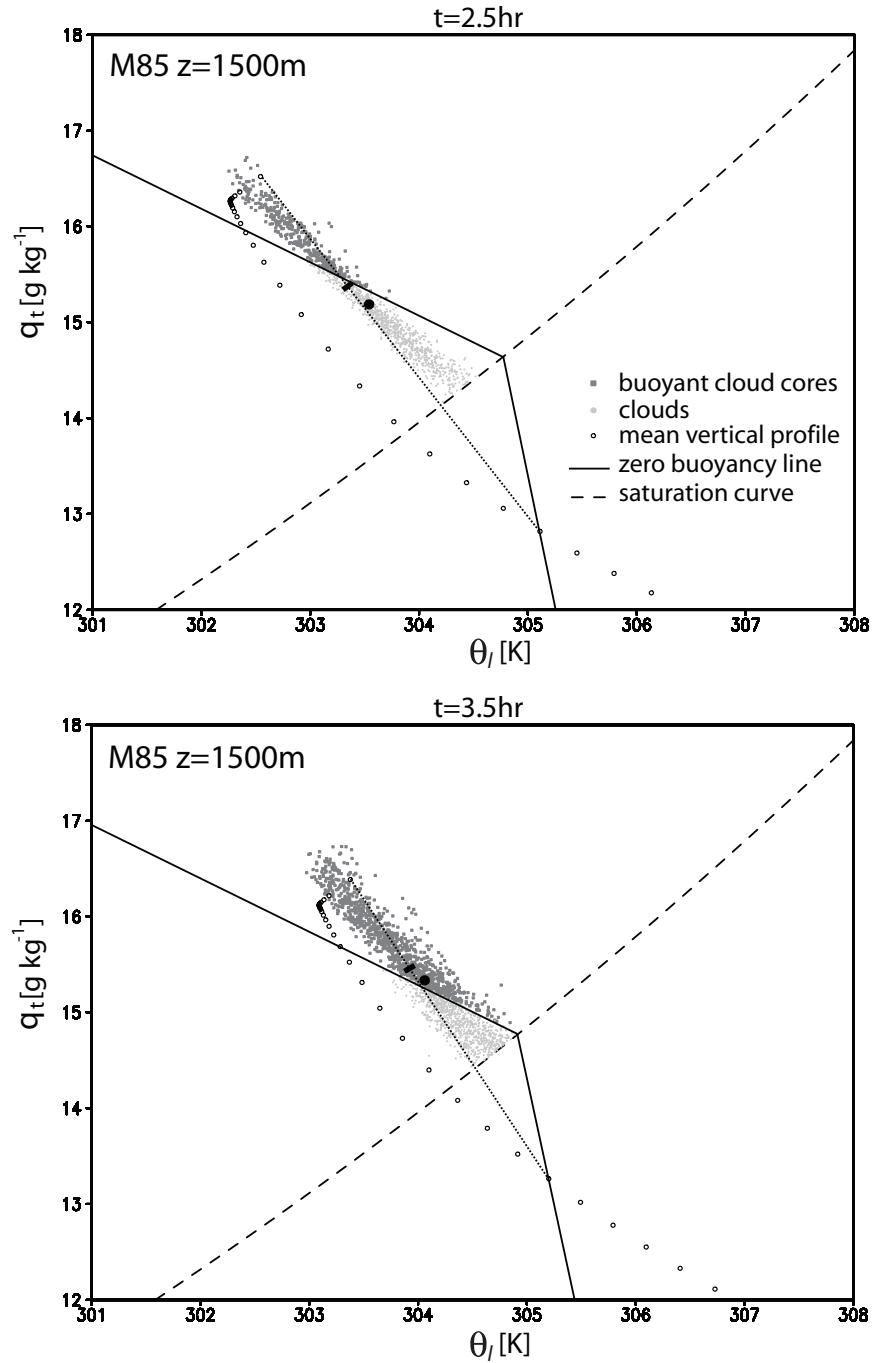


FIG. 9. The scatter plot of total water mixing ratio ( $q_t$ ) and the liquid water potential temperature ( $\theta_l$ ) of the cloudy points for experiment M85 before and after transition. The dotted line represents the line connecting the surface point and the observation level. The tick mark and the large dot represent the mean properties of the mixing model and the clouds.

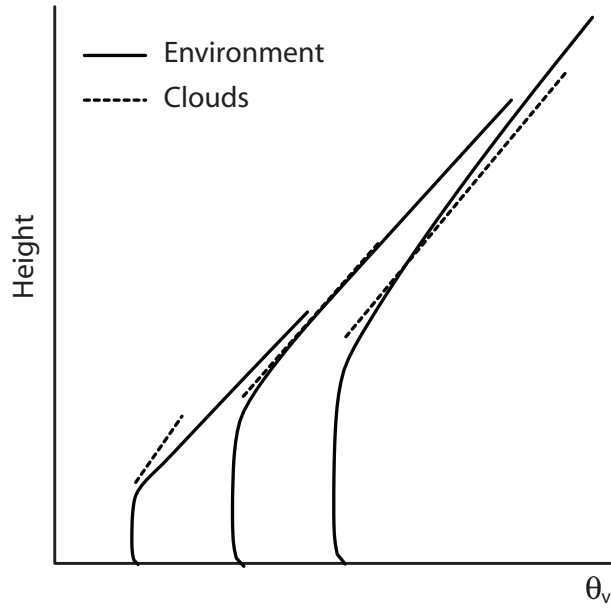


FIG. 10. A schematic illustration of transition from shallow to deep convection. The thick solid and dash lines represents the environment and cloud  $\theta_v$ , respectively. The environment  $\theta_v$  is averaged over the entire domain while the cloud  $\theta_v$  is averaged over cloudy points only. The three sets of profiles represent the profiles before, during and after the transition. See text for more detail.

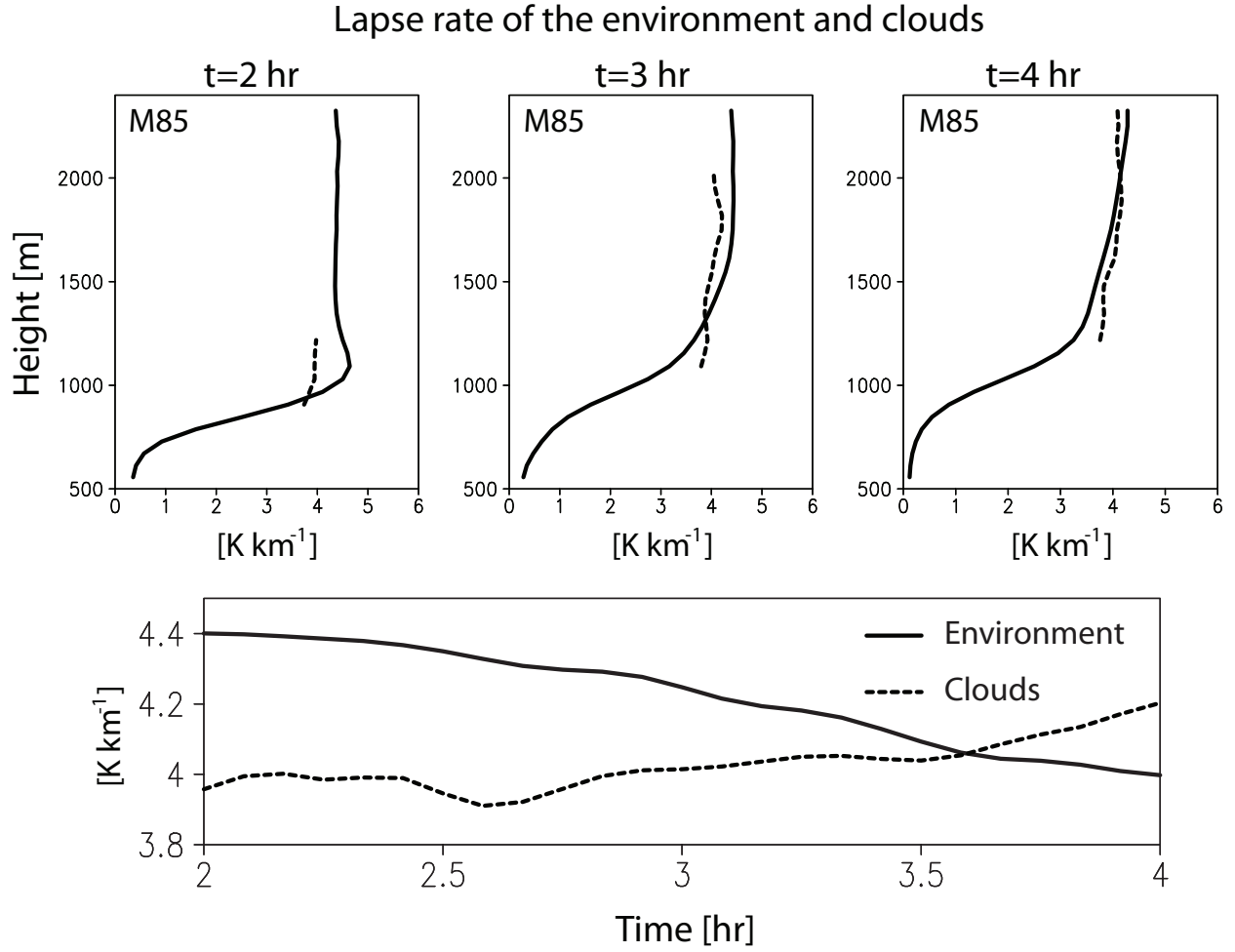


FIG. 11. The vertical profiles of the lapse rate of  $\theta_v$  in the shallow cumulus layer and the time evolution of the regressed lapse rate of  $\theta_v$  for experiment M85. The solid and dash lines represent the environment and the clouds, respectively.

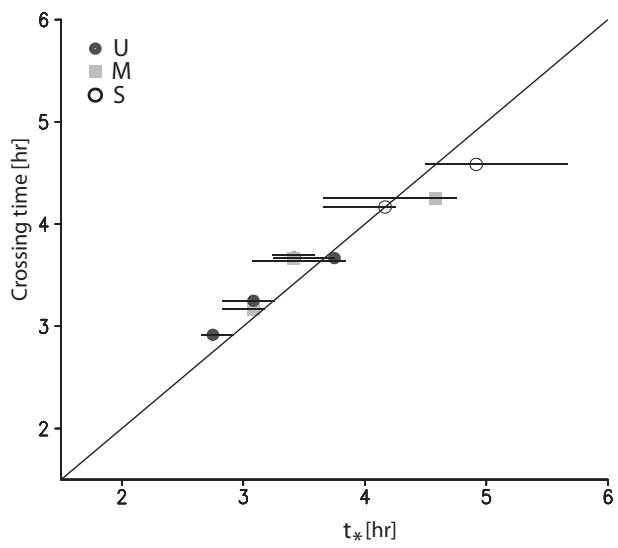


FIG. 12. Same as in Fig. 6 except for the transition time versus crossing time.

### Lapse rate of the environment and mixing model

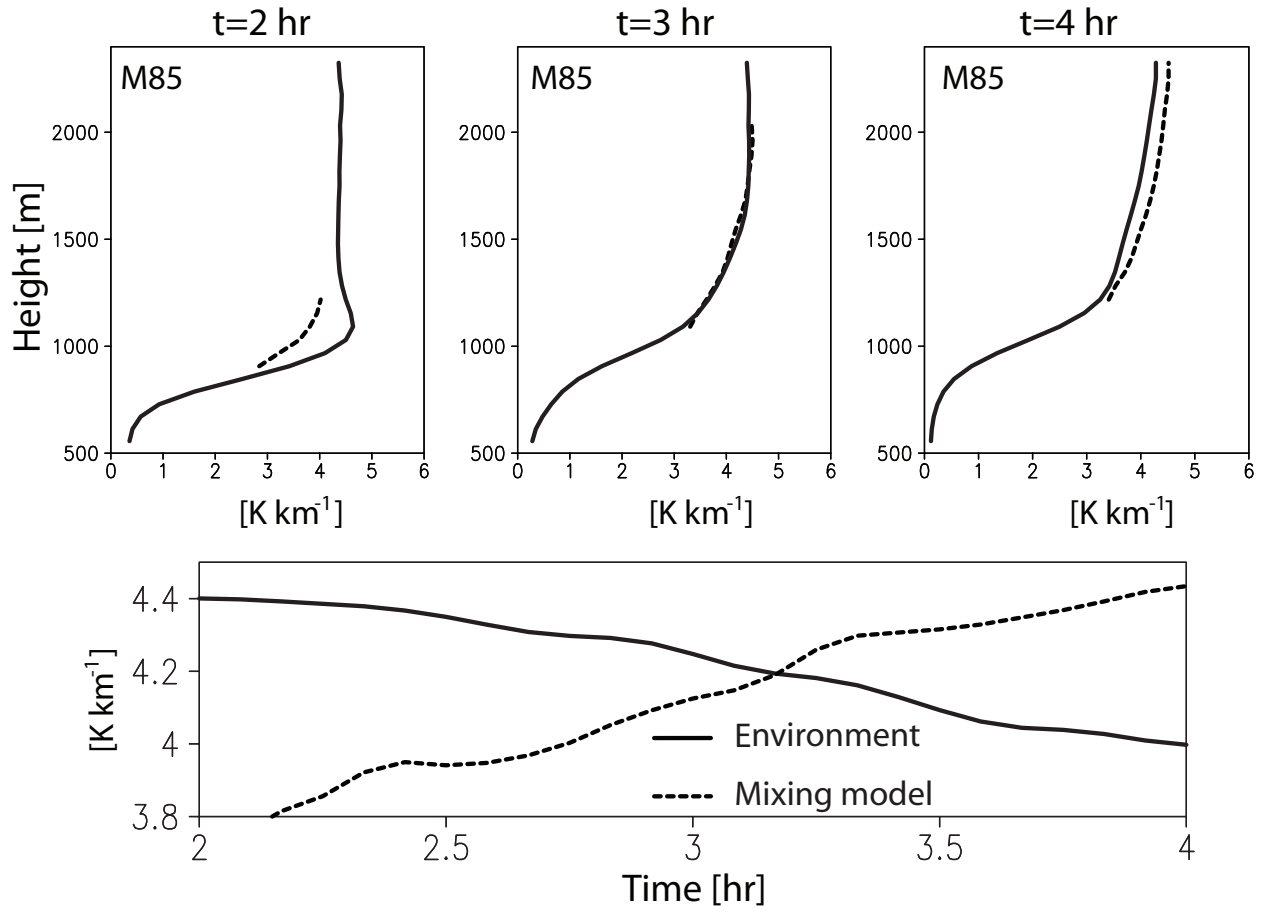


FIG. 13. As in Fig. 11 except for the mixing model.

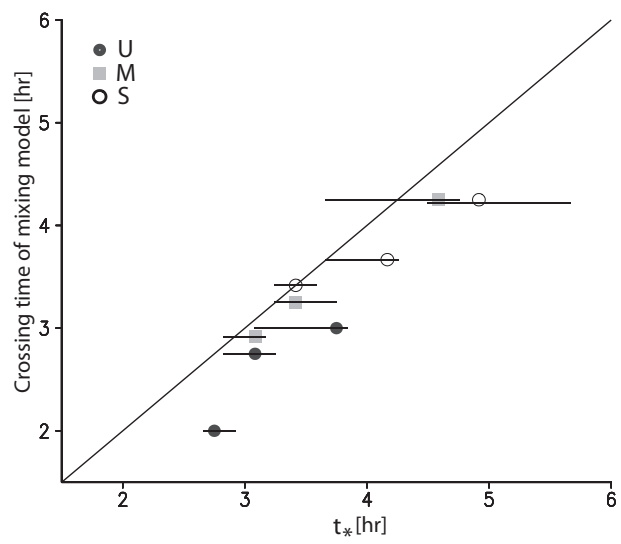


FIG. 14. As in Fig. 6 except for the transition time versus crossing time of mixing model.

## List of Tables

1	Sensitivity experiments. . . . .	45
2	Transition time (hr). . . . .	46

TABLE 1. Sensitivity experiments.

Experiments	80%	85%	90%	
U(unstable)	U80	U85	U90	U-class
M(control)	M80	M85	M90	M-class
S(stable)	S80	S85	S90	S-class
	X80	X85	X90	

TABLE 2. Transition time (hr).

Experiments	80%	85%	90%
U	3.8	3.1	2.8
M	4.6	3.4	3.1
S	4.9	4.2	3.4